Journal of Alloys and Compounds 520 (2012) 153–157

Contents lists available at SciVerse ScienceDirect

Journal of Alloys and Compounds

journal homepage: www.elsevier.com/locate/jallcom

Influence of covalency and anion polarization on magnetic and electronic properties of $ZnCr_{2-x}Ni_xSe_4$

Izabela Jendrzejewska[a,*], Paweł Zajdel[b], Tomasz Goryczka[c], Jerzy Goraus[b], Andrzej Kita[a], Tadeusz Mydlarz[d]

[a] University of Silesia, Institute of Chemistry, Szkolna 9, 40-006 Katowice, Poland
[b] University of Silesia, Institute of Physics, Uniwersytecka 4, 40-007 Katowice, Poland
[c] University of Silesia, Institute of Chemistry and Physics of Metals, Bankowa 12, 40-006 Katowice, Poland
[d] International Laboratory of High Magnetic Fields and Low Temperatures, Gajowicka 95, 53-529 Wrocław, Poland

ARTICLE INFO

Article history:
Received 19 October 2011
Accepted 30 December 2011
Available online 10 January 2012

Keywords:
Magnetically ordered materials
X-ray diffraction
Neutron diffraction
Magnetic measurements
EXAFS
Electronic band structure

ABSTRACT

Selenospinels ACr_2Se_4 form a broad class of materials with tunable properties, including thermoelectric, magnetoresistive and magnetocapacitance, related to the internal competing interactions.

On the basis of structural, magnetic and numerical studies of the cubic $ZnCr_{2-x}Ni_xSe_4$ ($x = 0.1$–0.3), we show that simple ionic model is not suitable for consistent description of the properties of the system. Although it may explain the systematic decrease of the saturation magnetic moments from $5.25\mu_B$/f.u. for $x = 0.1$ to $4.85\mu_B$/f.u. for $x = 0.3$, it fails to explain the trends in the lattice parameters and the chemical shifts of the absorption edges.

On the basis of the numerical calculations performed for $x = 0.2$, we obtain the agreement between the local magnetic moments on Cr ($3.18\mu_B$) and Ni ($-0.49\mu_B$) ions and the value obtained from neutron powder diffraction $2.65(3)\mu_B$ as well as saturation magnetization. However, the calculations and the consistence between different experiments require the presence of magnetic polarization on selenium $-0.11\mu_B$, which is usually neglected in ionic models.

1. Introduction

Chromium zinc selenide $ZnCr_2Se_4$ crystallizes in the $MgAl_2O_4$-type structure (space group 227, $Fd-3m$). Zinc and chromium are respectively tetrahedrally and trigonal antiprismatic (commonly called "octahedral" due to the ideal spinel case) co-ordinated within the cubic close packing of selenium atoms. The reported lattice parameter covers a wide range of values $a = 10.433$–10.524 Å [1–3], which is most likely caused by the non-stoichiometric samples. At room temperature, $ZnCr_2Se_4$ is a p-type semiconductor with a magnetic spiral structure ($k = 0.44(1)$ [4], $k = 0.456(1)$ [5], and $k = 0.465(10)$ [6], spiral angle $\phi \approx 42 \pm 1^\circ$), the Neel temperature 21 K and the paramagnetic Curie–Weiss temperature 115 K [6–9]. The magnetic properties have been found to result from multiple magnetic interactions, which included dominating nearest neighbor ferromagnetic (close to 90° Cr–Se–Cr angle) and more distant antiferromagnetic superexchange pathways [10]. There are usually altered by substitution of zinc or chromium with another 3d [11,12] metal leading to essential changes of the cation distribution and modifying physical properties of $ZnCr_2Se_4$.

So far the influence of nickel doping in chalcogenide spinels has been investigated in the sulphide $Zn_{1-x}Ni_xCr_2S_4$ [13], where nickel has been found as Ni^{2+} in the tetrahedral site has only. It coupled antiferromagnetically to chromium network and possessed a magnetic moment of $2.2 \pm 2.0\mu_B$.

The influence of low concentrations $x = 0.03$, 0.05 and 0.1 of nickel in the octahedral position has been studied in the case of $ZnCr_{2-x}Ni_xSe_4$ in the single crystal form [14,15] and the saturation magnetic moment was also found to decrease with Ni doping and samples with larger Ni content could only be synthesized in polycrystalline form.

Up to date, there are no complex studies of the $ZnCr_{2-x}Ni_xSe_4$. The presence of a nickel on the octahedral position has been already analyzed using X-Ray Absorption Spectroscopy and the results have been reported elsewhere [16]. In this paper, we present the details of the synthesis, analytical, magnetic, X-ray and neutron powder diffraction studies of the $ZnCr_{2-x}Ni_xSe_4$, with an aim to elucidate the effect of nickel substitution on the cation distribution and magnetic properties of these spinels.

2. Experimental

2.1. Synthesis

The compounds in $ZnCr_{2-x}Ni_xSe_4$-series, where $x = 0.1$–0.9 were prepared from the binary selenides (ZnSe, NiSe and Cr_2Se_3) and only the samples with $x = 0.1$–0.3

* Corresponding author.
E-mail address: izajen@wp.pl (I. Jendrzejewska).

0925-8388/$ – see front matter © 2012 Elsevier B.V. All rights reserved.
doi:10.1016/j.jallcom.2011.12.167

Table 1
Values of the paramagnetic effective Bohr magneton number and saturation magnetization per formula unit, asymptotic Curie temperature, Néel temperature and Curie constant per mol for $ZnCr_{2-x}Ni_xSe_4$ and the $ZnCr_2Se_4$.

Compound	μ_{eff} (μ_B/f.u.)	μ_{sat} (μ_B/f.u.)	Θ_{CW} (K)	C_M (K/mol)	T_N (K)
$Zn_{1.03(1)}Cr_{1.89(2)}Ni_{0.08(1)}Se_{3.89(3)}$	4.83 (2)	5.27	89.9 (2.2)	2.92 (3)	20
$Zn_{0.99(1)}Cr_{1.76(2)}Ni_{0.18(1)}Se_{3.94(3)}$	4.78 (2)	5.10	90.4 (2.2)	2.85 (3)	20
$Zn_{1.06(1)}Cr_{1.73(3)}Ni_{0.25(1)}Se_{3.76(3)}$	4.45 (2)	4.89	92.3 (2.3)	2.47 (3)	20
$ZnCr_2Se_4$ (31, 32)	5.47	5.74	115	3.54	21

were found to be a single spinel phase. The samples were sintered 4 times at 1073 K for 7 days.

2.2. Chemical composition

Chemical compositions of the obtained samples were determined using ICP-AES method (Inductively Coupled Plasma–Atomic Emission Spectrometry). The two-point spectrometer recalibration was applied and a separate standard for each element was used. The obtained results are presented in Table 1.

2.3. X-ray measurements

X-ray powder diffraction data of polycrystalline samples were collected using a Philips X-Pert (PW3050) diffractometer (CuK_α radiation) over an angular range of 2θ: 10/135°. The Rietveld refinement was performed with the FullProf suite [17] (Fig. 1).

2.4. Magnetic measurements

Magnetization isotherms at 4.2 K of the investigated compounds was studied in high magnetic stationary fields (up to 14 T) using an induction magnetometer with a Bitter-type magnet. The temperature was measured with a thermocouple of chromel-Au + 0.07%Fe with precision of 0.5 K. Magnetization isotherms for $ZnCr_{2-x}Ni_xSe_4$ are given in Fig. 2.

The magnetization measurements were carried out over the temperature range 1.8–300 K using a Quantum Design SQUID–based MPMSXL–5-type magnetometer (Fig. 3) with magnetic field of 0.5 T. The paramagnetic effective Bohr magneton number was calculated using the formula $\mu_{eff} = 2.83 : \overline{C_M}\mu_B$, where molar Curie constant was calculated from the Curie–Weiss law fit to points in the high temperature range 240–300 K.

The magnetic data for the polycrystalline compounds from the $ZnCr_{2-x}Ni_xSe_4$ systems, calculated per formula unit are given in Table 1. Value of transition temperature is estimated from the maximum of the magnetization curve. Although the paramagnetic asymptotic Curie temperature is positive, overall shape of the $M(T)$ is similar to the AF transition and for that reason is called Néel temperature T_N like for an antiferromagnet.

2.5. The neutron powder diffraction (NPD)

Neutron powder diffraction data were collected at BT-1 neutron powder diffractometer at the NIST Center for Neutron Research Gaithersburg, MD, USA, $\lambda = 2.0785$ Å. The instrument is described in the NCNR WWW site (http://www.ncnr.nist.gov/). The refinement was performed using FullProf suite [17] package and the magnetic phase was modeled using real space conical approach

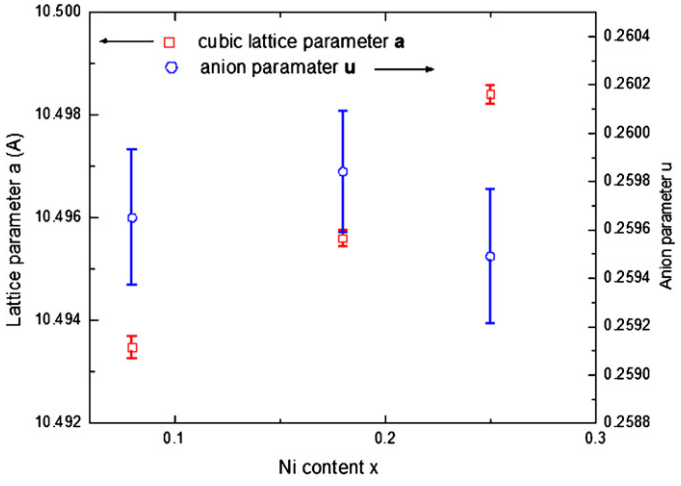

Fig. 1. The lattice and anion parameters for selected compounds vs. their measured nickel content.

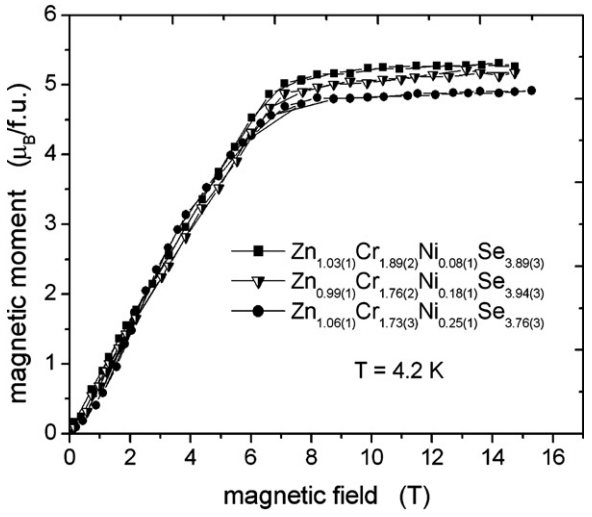

Fig. 2. Magnetization isotherms at 4.2 K for $ZnCr_{2-x}Ni_xSe_4$.

(JBT = 5). The Rietveld refinement of magnetic phase at 5 K (Fig. 4a) was performed using measured concentration of Ni. The obtained lattice parameter was equal to 10.48487(12) Å (at 5 K) (the error bar is statistical on 1σ level), anion parameter $u = 0.25963(6)$, magnetic moment on the octahedral site was $2.65(3)\mu_B$, propagation vector $k = 0.4573(3)$, which means that the pitch of helix is about 22.9 Å. Atomic displacement parameters (B_{iso}) were equal Zn, Cr/Ni, Se respectively 0.10(7) 1.11(7), 0.20(4). The agreement parameters were $\chi^2 = 3.69$, $R_{wp} = 10.9\%$, $R_{exp} = 5.7\%$, $R_B = 3.9\%$, $R_{mag} = 21.1\%$. During the fit it was impossible to decouple magnetic moments of Cr and Ni, so an average Cr^{+3}/Ni^{+2} ratio weighted magnetic form factor was used. The analysis revealed traces <6% of ZnSe (bottom set of Bragg positions). Temperature scans from 4 to 25 K showed decrease of the magnetic peak (Fig. 4b) and at 22 K no long range magnetic contribution was observed. Refinement of the propagation vector showed slow decrease with temperature (Fig. 4c). The changes of lattice and the anion parameter within this temperature range were negligible (within the fit error) and are not presented.

The structural parameters in the paramagnetic region at 50 K were found to be: $a = 10.4834(1)$ Å, $u = 0.25983(6)$ and the values of the isotropic atomic displacement parameters (B_{iso}) 0.569(132), 0.465(131), 0.182(40) Å^2 for Zn, Cr/Ni and Se

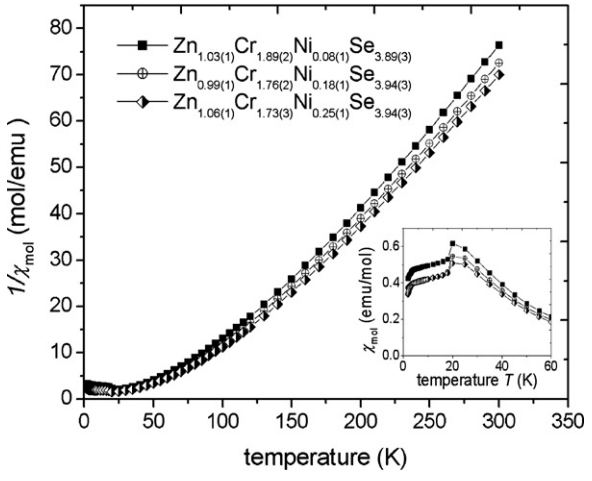

Fig. 3. Temperature dependence of the magnetic susceptibility for $ZnCr_{2-x}Ni_xSe_4$.

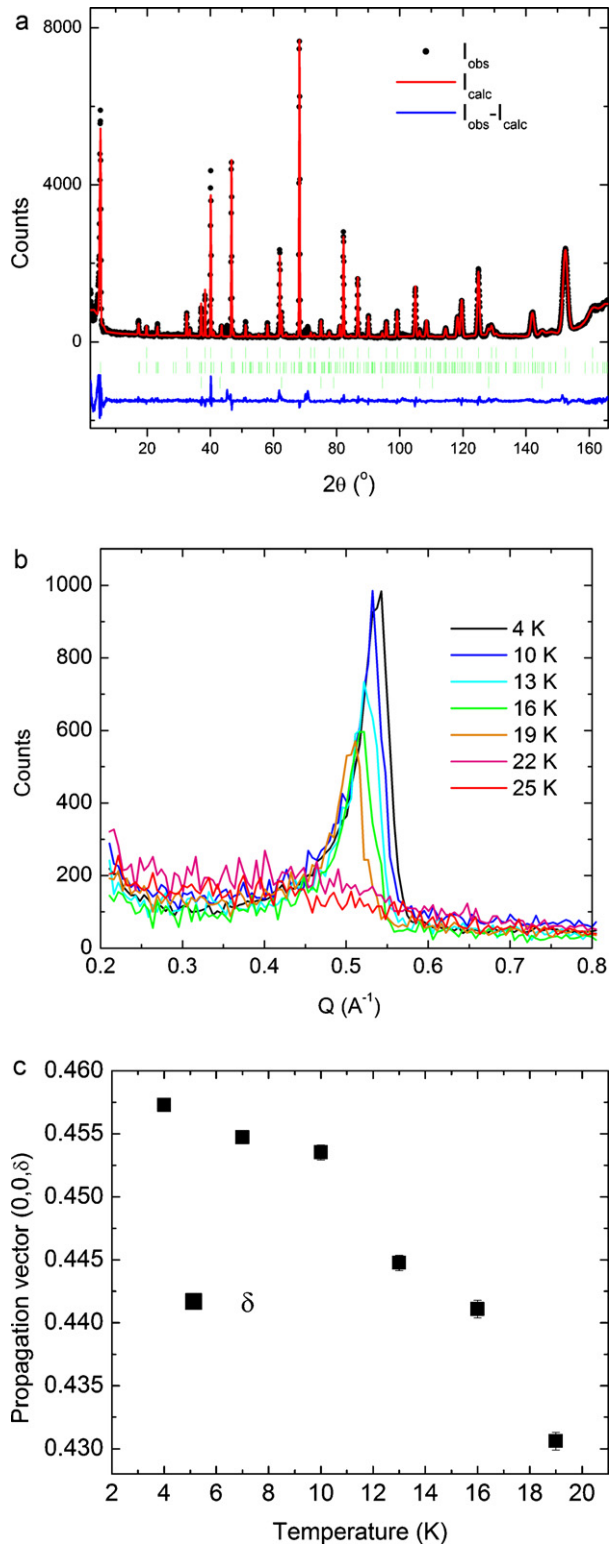

Fig. 4. (a) Rietveld refinement of helical magnetic structure of $ZnCr_{1.8}Ni_{0.2}Se_4$, (b) temperature evolution of the (0, 0, δ) peak and (c) the temperature dependence of the incommensurate modulation.

respectively. The observed negative thermal expansion of the lattice below 50 K is in agreement with the result for pure $ZnCr_2Se_4$ [18].

The surprisingly large value 1.11(7) of the B_{iso} of Cr/Ni at 5 K obtained from the NPD, was verified against the low temperature Extended Absorption Fine Structure (EXAFS) signal measurements, which provided information about the local structure around each of the sites. The Cr K and Ni K edges were recorded in the transmission mode at the 7.1 and 9.3 stations of the Daresbury Lab SRS. The experimental details

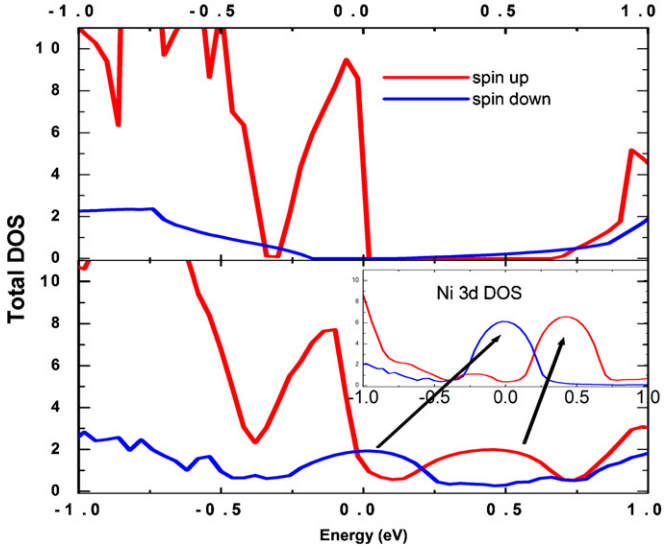

Fig. 5. Total DOS for $ZnCr_2Se_4$ (up) and $ZnCr_{1.8}Ni_{0.2}Se_4$ (down) – zoom of the Fermi energy shows that nickel 3d states are located exactly over the principal energy gap of $ZnCr_2Se_4$.

have been given in our previous report [16], where we have discussed the near edge region (XANES) spectra and the room temperature EXAFS. The modeling of EXAFS signal in 16 K and 30 K (plots in Supplemental Information) was performed using IFEFFIT(FEFF6L.02) and Artemis packages [19,20]. Unlike the B_{iso} in NPD, the EXAFS formula [21] caries rather the information the relative displacements projected on the scattering path of the central atom and the neighbor $\sigma^2{}_{12} \sim \langle(u_1 - u_2)^2\rangle$. However, it can be represented as $\langle u_1\rangle^2 + \langle u_2\rangle^2 - 2\langle u_1 u_2\rangle$, where the first 2 contributions should be in isotropic case roughly 1/3 of the respective $B_{iso}/8\pi^2$ and the last term is the correlated motion correction.

2.6. Full Potential Local Orbital (FPLO) calculations

Band structure calculations for $ZnCr_2Se_4$ and $ZnCr_{1.8}Ni_{0.2}Se_4$ solid solution performed using FPLO 5.00-20 (Full Potential Local Orbital) code with Coherent Potential Approximation (CPA) [22,23]. In our spin resolved, scalar relativistic calculations, we used exchange-correlation potential in the form proposed by Perdew–Wang [24] with Ceperley–Alder parametrization [25]. Partial densities of states of $ZnCr_{1.8}Ni_{0.2}Se_4$ were already reported in [16]. Fig. 5 presents details of the densities of states (DOS) in the proximity of Fermi energy for $ZnCr_2Se_4$ and $ZnCr_{1.8}Ni_{0.2}Se_4$ and the insert highlights the changes introduced by nickel 3d states in doped system. Although Mulliken analysis of partial charges is not completely reliable in open shell system like 3d metals, we have made a comparison of calculated charges between pure and doped cases, which results are presented in Table 2. The number of valence electrons is based on electrons from 3s, 3p, 3d, 4s and 4p shells.

3. Results and discussion

In the $ZnCr_{2-x}Ni_xSe_4$ system, spinel is the main product for $x = 0.1–0.3$ and no monoclinic phase is detected. The lattice parameters of the spinel phase increase from 10.4935(1) Å for $x = 0.08$ to 10.4994(7) Å for $x = 0.25$ with increasing Ni concentration (see Fig. 1), as expected, since the nominal ionic radius of Ni^{2+} (in octahedral site) is bigger than ionic radius of Cr^{3+} (see Table 3) [26].

For $ZnCr_{2-x}Ni_xSe_4$ systems, the dependence of lattice parameters on amount of Ni is linear and Vegard's law is obeyed (see Fig. 1).

It is known that cation distribution in a spinel structure depends on several conditions, two of which are stoichiometry and individual site preference of the cations. The Cr^{3+} ion has the highest octahedral site preference of all the 3d metals (69.5 kJ/mol) [26,27] and it is capable of forcing Ni^{2+} to move to tetrahedral sites like in $NiCr_2O_4$, where high Ni^{2+} concentration leads to the Jahn–Teller tetragonal deformation of the spinel structure [28]. On the other hand, other nickel chromium chalcogenides like $NiCr_2S_4$ and $NiCr_2Se_4$ form the monoclinic structure of Cr_3Se_4 (defected NiAs-type) [29], where nickel is octahedrally coordinated.

Table 2
Mullikan population analysis for the pure $ZnCr_2Se_4$ and $ZnCr_{1.8}Ni_{0.2}Se_4$.

	Zn (20)	Cr (14)	Cr 3d	Ni (18)	Ni 3d	Se (24)	Se 4p	Val. el. (per f.u.)
$ZnCr_2Se_4$								
Net	18.71	12.64	4.29	–	–	23.8	3.98	139.18
Gross	19.42	13.59	4.71	–	–	24.35	4.48	144.00
Mag. Mom.	0.03	3.20	3.10	–	–	**−0.11**	**−0.11**	6.00
$ZnCr_{1.8}Ni_{0.2}Se_4$								
Net	18.76	12.6	4.27	16.87	8.65	23.85	4.02	140.20
Gross	19.49	13.54	4.69	17.34	8.74	24.37	4.50	144.80
Mag. Mom.	0.02	3.18	3.08	**−0.49**	**−0.49**	**−0.11**	**−0.11**	5.20

The 'Net' charge is outer electrons belonging only to given atom. The 'Gross' number contains also contribution from half of hybridized electrons. Magnetic moment is a total per atom. Last column gives number of valence electrons and magnetic moment per formula unit. The values under the element name give number of valence electrons at the beginning of calculation.
Negative numbers in bold denote polarization opposite to Cr.

When the tetrahedral site in spinel is fully occupied by zinc, nickel ions are forced to share the octahedral positions with chromium. Additionally nickel, like chromium has a strong preference for the octahedral site (37.7 kJ/mol) [26,27]. The increase of the lattice parameter with increasing Ni content is consistent with Ni in the octahedral position (close to Ni^{2+}) state, since it is the only reported configuration that has radius larger than the one of Cr^{3+} ion. In [16] we showed that the analysis of the Extended X-Ray Absorption Fine Structure (EXAFS) data fully agrees with the octahedral coordination of nickel. Also, the chemical shift of Ni K edge in $NiCr_2Se_4$ and $ZnCr_{1.8}Ni_{0.2}Se_4$, implied that nickel, except the common coordination, has in both cases a similar valence.

However, this must be treated with certain care due to covalency of the system. Indeed, the differences between electrons belonging to only one atom ("Net" population) and shared ("Gross") given in Table 3 indicate that, for example for Cr, a larger charge is shared in covalent bond ($13.54 - 12.6 \approx 0.9$) than is transferred out from the Cr ($14.0 - 13.6 \approx 0.4$). That points toward breaking of the pure ionic approximation. Also the comparison of doped and pure cases, reveals that Ni doping almost does not change the per atom charges.

Calculated magnetic moments in Bohr magnetons per atom for Cr, Ni and Se are respectively 3.18, −0.49, and −0.11. The predicted value of moment on B-site based on the total contribution from an average Cr/Ni atom (1.76Cr and 0.18Ni) is $2.75\mu_B$, which is close to $2.65(3)\mu_B$ obtained from neutron diffraction. The negative polarization of nickel can be also seen in the theoretical DOS (Fig. 5), where Ni 3d spin-down states are lower in energy than their 3d copies, split by about 0.5 eV. The location of nickel 3d states at Fermi level explains also the increased n-type character of the material [15]. Although the obtained band structure has a metallic character, we note that it is calculated with an ideal alloy approximation. In real structure it would result with metallic islands around Ni ions separated by semiconducting matrix.

It is worth commenting that the calculated magnetic moment of Cr 3d band alone is $3.08\mu_B$, while for total Cr atom is $3.18\mu_B$, which means the remaining $0.1\mu_B$ must come from polarized 4sp orbitals.

We have to note also the contribution of selenium anion to the magnetism. Although 'per atom' magnetic contribution of selenium is 5 times smaller than Ni, on 'per molecule' level it is two times larger. Indeed, Ni share is $0.18 \times -0.49 = -0.09\mu_B$ and Se is $4 \times -0.11 = -0.44\mu_B$. This has significant consequences for interpretation of saturation magnetization. The theoretical value of M_{sat} calculated in the FPLO is $5.2\mu_B$, which agrees quite well with the experimental $5.1\mu_B$. Now, a standard interpretation of the magnetization based on an ionic model of bonding, which usually assumes magnetism only on Cr and Ni cations, would be done as follows: Cr^{3+} would be assumed to have moment of $3\mu_B$ and the resulting moment on nickel would be $M_{Ni} = (M_{total} \times n_{Cr} \times M_{Cr})/n_{Ni} = (5.2 - 1.8 \times 3)/0.2 = -1\mu_B$. Such value would be interpreted as presence of low spin Ni^{3+} ion, which is incompatible with the increase of lattice parameter due to small ionic radius of Ni^{3+} (Table 3) and the XAFS results [16].

We argue that interpretation consistent with: expansion of the lattice, the position and shape of absorption edge as well as our calculations must be based on more covalent than ionic bond in $ZnCr_2Se_4$ and presence of nickel in lower valence states.

Similar reasoning is not necessary in the case of parent $ZnCr_2Se_4$, where the saturation magnetic moment $5.9\mu_B$ [30–32] lies very close to $6\mu_B$/f.u., which is a predicted value for spin only contribution of two Cr ions in high spin electron configuration $3d^3$ ($S = 3/2$). The small difference has been attributed to the covalency effects and hybridization of chromium 3d orbitals with anion 4p states.

Also, as it has been already shown in the case of $MgAl_2O_4$:Ni^{2+} [33], nickel ions prefer to occupy octahedral sites in spinel as Ni^{2+} not Ni^{3+}. In our case, the increased covalency of the chemical bond in selenide does not allow us to say the nickel is also in Ni^{2+} state like in the oxide, since we cannot assume a full electron transfer from nickel to selenium. However, the similarity of the chemical shift of the Ni K absorption edge [15], between $NiCr_2Se_4$ and $ZnCr_{1.8}Ni_{0.2}Se_4$ suggest that Ni in both cases is in a similar charge state. We must note that the calculations show that charge state of nickel is $3d^{8.7+}$ [16], which is nominally closer to Ni^+ but, as we said earlier, such configuration cannot be treated as purely ionic. On the basis of the previous discussion we will only concentrate on nickel close to Ni^{2+}.

As can be seen in Table 1 (obtained from Figs. 2 and 3) the magnetization in saturation state at liquid helium temperature decreases with increasing Ni substitution, while the paramagnetic Curie temperature remains unchanged. This indicates that despite the decreased saturation the nearest neighbor coupling remains unchanged.

The temperature dependence of magnetic moment is characteristic for the first order phase transition and the incommensurate pitch value δ at 5 K agrees within the error with the one of pure $ZnCr_2Se_4$. At 19 K, we still observe a well developed magnetic order with $2\mu_B$ per Cr ion, which disappears at 22 K. This is consistent with the $M(T)$ magnetization curve going through maximum at 20 K. The temperature evolution of propagation vector closely follows the value of magnetic moment The lattice parameter a

Table 3
The ionic radii and site-preference-energy E_v for ions of zinc, nickel and chromium (26, 27).

Ion	Ionic radius (Å)	E_v (kJ/mol K)
Zn^{2+}	0.60	−132.3
Ni^{2+}	0.55 (in tetrahedral site) 0.69 (in octahedral site)	37.7
Ni^{3+}	0.56 (LS)/0.60 (HS)	–
Cr^{3+}	0.62	69.5
Cr^{2+}	0.73 (LS)/0.80 (HS)	–

LS – low spin and HS – high spin.

and anion parameter u do not follow a similar trend and remain constant within fit error. Such behavior of k indicates that the strength of the interplanar magnetic coupling depends on the value of the ordered magnetic moment, which would point toward magnetoelastic effect as a possible cause. On the other hand, magnetostriction, would be expected to similarly affect the structural parameters, which we do not observe but we cannot exclude the possibility that the changes in a and u are smaller than our resolution.

Here we shall comment on the large value 1.11(7) of the B_{iso} of Cr/Ni at 5 K obtained from the NPD. The Ni K edge at 16 K and 30 K and Cr K edge at 30 K were modeled as single scattering paths from the transition atom to 6 neighboring Se ions using structural data from NPD at 16 K and 25 K. The fits were performed with multiple weights k^2, k^3 with amplitude correction factor **amp**, energy shift $\mathbf{\Delta E}$, distance correction $\mathbf{\Delta r}$ and the $\boldsymbol{\sigma^2}_{TM-Se}$ as parameters. Their respective values obtained for 16 K/30 K fits were: 0.6(1)/0.6(1), −1.9(1.6)/−1.8(1.8) eV, −0.076(5)/−0.078(6) Å, 0.0029(5)/0.0026(6) Å^2. For comparison, the Cr K edge fit at 30 K resulted in 0.86(4), 3.8(7) eV, 0.004(2) Å, 0.0026(3) Å^2 respectively. The Cr K 16 K dataset was not fully recorded due to technical problem. The refined values of $\sigma^2{}_{NiSe}$ at 16 K and 30 K are comparable to each other within the one uncertainty bar, which does not confirm the significant increase observed in NPD. The rough – excluding correlated motion correction – estimate of B_{iso}Ni + B_{iso}Se at 5 K would be $3 \times 0.029 \times 8\pi^2 = 0.69$, which is much smaller than the refined 1.1.

In this situation, there are 2 possible answers contributing to the large value of B_{iso} Cr/Ni:

- that such large value of B_{iso} Cr/Ni is just an artifact of the refinement, due to short range of reciprocal space covered by the long wavelength diffractogram. In fact, fixing the value of B_{iso} Cr/Ni at 0.3 increases χ^2 only from 3.7 to 3.9;
- the distance TM–Se remains the same but the Se–TM–Se dihedral angle changes, which increases the atomic displacement perpendicular to the bond direction.

The first explanation is more probable.

4. Conclusions

The applied preparative method allowed to obtain quaternary compounds with general formula $ZnCr_{2-x}Ni_xSe_4$ ($x = 0.08$–0.25) and spinel structure (space group $Fd{-}3m$). The lattice parameters increased with the increasing Ni concentration, which is consistent with the presence of nickel in the octahedral position as was reported earlier (16). The magnetic moments: effective and in saturation, decrease with increasing Ni-amount in the series. This is caused by two factors: the replacement of Cr-ions by nickel, which possess smaller magnetic moment and opposite polarization of Ni and Cr. The paramagnetic asymptotic Curie–Weiss temperature values (Θ_{CW}) for $ZnCr_{2-x}Ni_xSe_4$-series are similar, what proves that dominating interactions between nearest neighbors remain ferromagnetic.

Comparison the increased covalent character of the bond system requires that in analysis of the saturated magnetic moment one must also include the influence of polarized selenium anions.

Acknowledgments

Synchrotron studies were done under CCLRC Direct Access project SRS45295 and funds from the EU FP6. JG acknowledges Polish Ministry of Science and Higher Education Project No. N N202 032137. PZ wants to thank Dr. S. Fiddy from the DL staff and Dr. hab. H. Duda from U. of Silesia for help during the experiment.

Appendix A. Supplementary data

Supplementary data associated with this article can be found, in the online version, at doi:10.1016/j.jallcom.2011.12.167.

References

[1] P.K. Baltzer, H.W. Lehmann, M. Robbins, Phys. Rev. Lett. 15 (1965) 493–495.
[2] A. Menth, A.R. von Neida, L.K. Schick, D.L. Malm, J. Phys. Chem. Solids 33 (1972) 1338–1341.
[3] 2001 PDF-2 database – International Centre for Diffraction Data.
[4] F. Yokaichiya, A. Krimmel, V. Tsurkan, I. Margiolaki, P. Thompson, H.N. Bordallo, A. Buchsteiner, N. Stuesser, D.N. Argyriou, A. Loidl, Phys. Rev. B 79 (2009) 064423.
[5] J. Akimitsu, K. Siratori, G. Shirane, M. Iizumi, T. Watanabe, J. Phys. Soc. Jpn. 44 (1) (1978) 172–180.
[6] P.R. Plumier, J. Phys. 27 (1966) 213–219.
[7] P.R. Plumier, C.R. Acad. Sci. Paris 260 (1965) 3348–3350.
[8] H.D. Lutz, G.P. Görler, F. Feher, Z. Naturforsch. 26A (1971) 1238–1240.
[9] O.V. Ershov, A.A. Minakov, V.G. Veselago, Sov. Phys. Solid State 26 (1984) 929–930.
[10] K. Dwight, N. Menyuk, Phys. Rev. 163 (2) (1967) 435–443.
[11] I. Jendrzejewska, J. Alloys Compd. 305 (2000) 90–92.
[12] E. Maciążek, A. Molak, T. Goryczka, J. Alloys Compd. 441 (2007) 222–230.
[13] H. Itoh, K. Motida, S. Miyahara, J. Phys. Soc. Jpn. 43 (1977) 854–856.
[14] I. Jendrzejewska, A. Waśkowska, T. Mydlarz, J. Alloys Compd. 327 (2001) 73–77.
[15] H. Duda, I. Jendrzejewska, T. Groń, S. Mazur, P. Zajdel, A. Kita, J. Phys. Chem. Solids 68 (2007) 80–86.
[16] P. Zajdel, I. Jendrzejewska, J. Goraus, H. Duda, T. Goryczka, A. Kita, Radiat. Phys. Chem. 80 (2011) 1008–1013.
[17] J.R. Rodriguez-Carvajal, Physica B 192 (1993) 55–69.
[18] R. Kleinbereger, R. de Kouchkovsky, C.R. Acad. Sci. 262 (1966) 628–630.
[19] M. Newville, J. Synchrotron Radiat. 8 (2001) 322–324.
[20] B. Ravel, M. Newville, J. Synchrotron Radiat. 12 (4) (2005) 537–541.
[21] J.J. Rehr, R.C. Albers, Rev. Mod. Phys. 72 (3) (2002) 621–651.
[22] K. Koepernik, H. Eschrig, Phys. Rev. B 59 (1999) 1743–1757.
[23] K. Koepernik, B. Velicky, R. Hayn, H. Eschrig, Phys. Rev. B 55 (1997) 5717–5729.
[24] J.P. Perdew, Y. Wang, Phys. Rev. B 45 (1992) 13244–13249.
[25] D.M. Ceperley, B.J. Alder, Phys. Rev. Lett. 45 (1980) 566–569.
[26] R.D. Shannon, Acta Cryst. A32 (1976) 751–767.
[27] A. Weiss, H. Witte, Kristallstrukture und chemische Bindung, Verlag Chemie, Weinheim, Germany, 1983.
[28] T. Armbuster, G.A. Lager, J. Ihringer, F.J. Rotella, J.D. Jorgensen, Z. Kistallogr. 162 (1983) 8–10.
[29] F. Jellinek, Acta Crystallogr. 10 (1957) 620–628.
[30] G. Bush, B. Magyar, O. Vogt, Solid State Commun. 7 (1969) 509–510.
[31] P. Gibart, M. Robbins, V.G. Lambrecht Jr., J. Phys. Chem. Solids 34 (1973) 1363–1368.
[32] J. Hemberger, H.-A. Krug von Nidda, V. Tsurkan, A. Loidl, Phys. Rev. Lett. 98 (2007), 147203-1–147203-4.
[33] M.G. Brik, N.M. Avram, C.N. Avram, C. Rudowicz, Y.Y. Yeung, P. Gnutek, J. Alloys Compd. 432 (2007) 61–68.